

A Direct-Forcing Immersed Boundary Projection Method for Thermal Fluid-Solid Interaction Problems

Cheng-Shu You¹, Po-Wen Hsieh² and Suh-Yuh Yang^{3,*}

¹ Department of Applied Mathematics, Feng Chia University, Xitun District, Taichung City 40724, Taiwan

² Department of Applied Mathematics, National Chung Hsing University, South District, Taichung City 40227, Taiwan

³ Department of Mathematics, National Central University, Jhongli District, Taoyuan City 32001, Taiwan

Received 11 May 2021; Accepted (in revised version) 28 November 2021

Abstract. In this paper, we develop a direct-forcing immersed boundary projection method for simulating the dynamics in thermal fluid-solid interaction problems. The underlying idea of the method is that we treat the solid as made of fluid and introduce two virtual forcing terms. First, a virtual fluid force distributed only on the solid region is appended to the momentum equation to make the region behave like a real solid body and satisfy the prescribed velocity. Second, a virtual heat source located inside the solid region near the boundary is added to the energy transport equation to impose the thermal boundary condition on the solid boundary. We take the implicit second-order backward differentiation to discretize the time variable and employ the Choi-Moin projection scheme to split the coupled system. As for spatial discretization, second-order centered differences over a staggered Cartesian grid are used on the entire domain. The advantages of this method are its conceptual simplicity and ease of implementation. Numerical experiments are performed to demonstrate the high performance of the proposed method. Convergence tests show that the spatial convergence rates of all unknowns seem to be super-linear in the 1-norm and 2-norm while less than linear in the maximum norm.

AMS subject classifications: 35Q79, 65M06, 76D05, 76M20

Key words: Fluid-solid interaction, heat transfer, direct-forcing method, immersed boundary method, projection scheme.

*Corresponding author.

Emails: cscopy@fcu.edu.tw (C.-S. You), pwhsieh@nchu.edu.tw (P.-W. Hsieh), syyang@math.ncu.edu.tw (S.-Y. Yang)

1 Introduction

In this paper, we will develop a direct-forcing immersed boundary approach combined with the Choi-Moin projection scheme for numerical simulations of heat transfer in the thermal fluid-solid interaction (TFSI) problems. We particularly emphasize the accurate imposition of the Neumann thermal boundary condition on the immersed solid boundary. It is well known that the understanding of the interaction dynamics between fluid and structure is of great importance in many applications of science and engineering. A commonly used numerical approach for simulating the flow dynamics with complex boundaries is based on the body-fitted discretization. The incompressible Navier-Stokes equations are spatially discretized over an unstructured grid that conforms to the immersed structure boundaries, and thus the boundary conditions can be imposed directly. However, due to the geometrical complexity encountered in the problems, it is still challenging and computationally expensive to simulate the dynamics of fluid-structure interaction problems using the conventional body-fitted approach.

To efficiently address the complex fluid-solid interaction (FSI) problems, one often appeals to the Cartesian grid-based non-boundary conforming methods. Such kind of techniques based on Cartesian grids provides many advantages over the body-fitted methodology, such as simplicity in grid generation, savings in computation time and memory usage, and straightforward parallelization. Consequently, they have been extensively studied in the analysis of FSI problems in science and engineering applications. In the past decades, the so-called immersed boundary (IB) method, which was first developed by Peskin [30, 31] in the 1970s, is one of the powerful Cartesian grid-based methods that is frequently used for simulating the dynamics of FSI problems, even with moving boundaries. In the IB method, the immersed structure exerts a boundary force on the fluid, and the interaction between structure and fluid can be represented by a contribution to the forcing term in the fluid equations by means of the Dirac delta function. Instead of generating a boundary-fitted grid to the immersed boundary at each time step, the spatial discretization of the IB method is implemented over Cartesian grids for the entire domain, and the immersed boundary is discretized by a set of Lagrangian marker points that are not constrained to lie on the grids. For more details we refer the reader to e.g., [18, 24, 31] and many references cited therein. This paper aims to study a popular variant of the IB method, called the direct-forcing IB method, see e.g., [3, 4, 8, 9, 12, 14–17, 20–23, 25, 27–29, 33–36, 38, 40]. We note that most of the direct-forcing IB methods reported in the literature have been directed toward analyzing fluid flow problems. However, in the present work, we are mainly concerned with heat transfer phenomena in TFSI problems.

In this paper, we will develop an efficient direct-forcing IB projection method for simulating heat transfer in the TFSI problems. This direct-forcing approach was first considered by Kajishima et al. [16, 17] in the 2000s for FSI problems and has been further studied in many applications, see, e.g., [3, 14, 27], and references cited therein. The underlying idea of this direct-forcing approach for addressing the TFSI problems is that we first

treat the solid as made of fluid and then introduce a virtual force to the incompressible Navier-Stokes equations for velocity and pressure and a virtual heat source to the energy transport equation for temperature. More specifically, the virtual force distributed only on the solid region is appended to the momentum equation to make the region behave like a real solid body and exactly satisfy the prescribed velocity. On the other hand, the virtual heat source located inside the solid region near the boundary is added to the energy transport equation to impose either the temperature (Dirichlet) or the heat flux (Neumann) boundary conditions on the immersed solid boundary. In the conventional direct-forcing approach, the Dirichlet boundary condition for temperature can be easily imposed. However, it seems not easy to accurately impose the heat flux boundary condition owing to their differences in nature [3, 29, 32, 37]. Therefore, the interpolation algorithms for enforcing the heat flux boundary condition have less been reported before in the literature. In this paper, to successfully extend this approach, we will propose a simple and clever interpolation technique for accurately imposing the Neumann thermal boundary condition on the immersed solid boundary.

After introducing these two virtual forcing terms, we will take the implicit second-order backward differentiation to discretize the time variable and employ the Choi-Moin projection scheme [5] to split the nonlinear coupled system. As for the spatial discretization, second-order centered differences over a staggered Cartesian grid will be used to discretize the space variable on the entire domain, including the solid body region. In particular, the virtual force and virtual heat source can be explicitly specified in the solution procedure. We can find that the proposed method is not only conceptually simple but also easy to implement, without using any Dirac delta functions that are necessary for the traditional IB methods. To validate this method's simplicity and efficiency, we will perform numerical experiments on several TFSI problems. The considered benchmark problems include the natural heat convection in a square enclosure with a heated cylinder [3], the natural heat convection in an annulus [11, 37, 39], the forced heat convection without buoyancy over a cylinder with constant heat flux [11], and the mixed heat convection with buoyancy in the lid-driven cavity with an embedded cylinder [19, 37]. These numerical examples show the high capability of the proposed method in solving complex-geometry heat transfer phenomena in the TFSI problems. Moreover, convergence tests show that the spatial convergence rates of all unknowns seem to be super-linear in the 1-norm and 2-norm while less than linear in the maximum norm. We also find that our numerical results are in excellent agreement with the previous works in the literature [3, 11, 19, 37, 39].

The remainder of this paper is organized as follows. In Section 2, we introduce the governing equations of the TFSI problem. In Section 3, we propose the direct-forcing IB projection method. Several numerical experiments are presented in Section 4. A summary and conclusions are given in Section 5. Finally, some technical details of Section 3 are provided in the Appendix section.

2 The governing equations of the TFSI problem

We consider a two-dimensional bounded fluid domain $\Omega \subset \mathbb{R}^2$ that encloses a single rigid solid body positioned at $\overline{\Omega}_s(t)$ with a prescribed velocity $\mathbf{u}_s(t, \mathbf{x})$. The cases of the three-dimensional fluid domain and multiple solid bodies can be treated similarly. Following the idea of the direct-forcing IB projection approach [16, 17], we first regard the solid as made of fluid and then introduce a virtual force \mathbf{F} distributed only on the solid body region $\overline{\Omega}_s$ that enforces the region to behave like a real solid body and to exactly satisfy the prescribed velocity:

$$\mathbf{u} = \mathbf{u}_s \quad \text{in } (0, T) \times \overline{\Omega}_s, \quad (2.1)$$

where $(0, T)$ is the time interval under consideration. We introduce a virtual heat source E which is located inside the solid region but near the boundary to help impose one of the following boundary conditions for temperature θ on the immersed solid boundary:

- Dirichlet thermal boundary condition:

$$\theta = \theta_s \quad \text{on } (0, T) \times \partial\Omega_s, \quad (2.2)$$

- Neumann thermal boundary condition:

$$-\kappa \frac{\partial \theta}{\partial \mathbf{n}} = Q_s \quad \text{on } (0, T) \times \partial\Omega_s, \quad (2.3)$$

where θ_s and Q_s are respectively the prescribed temperature and heat flux on the boundary $\partial\Omega_s$, \mathbf{n} is the outward unit normal vector to $\partial\Omega_s$ and $\kappa > 0$ is the thermal conductivity. The virtual force \mathbf{F} will be appended to the momentum equation of the incompressible Navier-Stokes equations to accommodate the interaction between the solid and fluid. In contrast, the virtual heat source E will be added to the energy transport equation to address the thermal boundary conditions. At this moment, we do not know how to specify the virtual force \mathbf{F} and the virtual heat source E , but we will specify them later in their time-discrete versions in the solution procedure.

In what follows, for simplicity, we assume that there is no body force for the incompressible viscous fluid and no heat source of the heat equation. Let \mathbf{u} be the velocity field, p the pressure, θ the temperature, and let $\mathbf{e} = (0, 1)^\top$ be the unit vector in the vertical direction. Then the governing equations of the TFSI problem with virtual force \mathbf{F} and virtual heat source E can be posed as follows:

$$\frac{\partial \mathbf{u}}{\partial t} - P_1 \nabla^2 \mathbf{u} + (\mathbf{u} \cdot \nabla) \mathbf{u} + \nabla p - P_2 \theta \mathbf{e} = \mathbf{F} \quad \text{in } (0, T) \times \Omega, \quad (2.4a)$$

$$\nabla \cdot \mathbf{u} = 0 \quad \text{in } (0, T) \times \Omega, \quad (2.4b)$$

$$\mathbf{u} = \mathbf{u}_s \quad \text{in } (0, T) \times \overline{\Omega}_s, \quad (2.4c)$$

$$\mathbf{u} = \mathbf{u}_0 \quad \text{in } \{0\} \times \overline{\Omega}, \quad (2.4d)$$

$$\mathbf{u} = \mathbf{u}_b \quad \text{on } (0, T) \times \partial\Omega, \quad (2.4e)$$

$$\frac{\partial \theta}{\partial t} - P_3 \nabla^2 \theta + \mathbf{u} \cdot \nabla \theta = E \quad \text{in } (0, T) \times \Omega, \quad (2.4f)$$

$$\theta = \theta_0 \quad \text{in } \{0\} \times \bar{\Omega}, \quad (2.4g)$$

$$\theta = \theta_b \quad \text{on } (0, T) \times \partial \Omega, \quad (2.4h)$$

$$\theta = \theta_s \quad \text{on } (0, T) \times \partial \Omega_s \quad \text{or} \quad -\kappa \frac{\partial \theta}{\partial \mathbf{n}} = Q_s \quad \text{on } (0, T) \times \partial \Omega_s, \quad (2.4i)$$

where the initial and the boundary functions, \mathbf{u}_0 , θ_0 , \mathbf{u}_b , and θ_b , are all prescribed.

The dimensionless parameters P_1 , P_2 , and P_3 in the TFSI problem (2.4a)-(2.4i) are defined according to the scaling and depending on the problem under analysis [3, 29]. In this paper, we consider the following three different cases:

- For natural heat convection, we have

$$P_1 = Pr, \quad P_2 = RaPr, \quad P_3 = 1, \quad (2.5)$$

- For forced heat convection without buoyancy, we have

$$P_1 = \frac{1}{Re'}, \quad P_2 = 0, \quad P_3 = \frac{1}{RePr'}, \quad (2.6)$$

- For mixed heat convection with buoyancy, we have

$$P_1 = \frac{1}{Re'}, \quad P_2 = \frac{Gr}{Re^2}, \quad P_3 = \frac{1}{RePr'}, \quad (2.7)$$

where $Pr := \nu / \alpha$ is the Prandtl number, $Ra := GrPr$ is the Rayleigh number, $Re := (UL_c) / \nu$ is the Reynolds number, and Gr is the Grashof number which is defined as

$$Gr := \begin{cases} \frac{g\beta L_c^3}{\nu^2} (T_w - T_0) & \text{for natural convection case (2.5),} \\ \frac{g\beta L_c}{U^2} (T_w - T_0) \left(\frac{UL_c}{\nu}\right)^2 & \text{for mixed convection case (2.7).} \end{cases} \quad (2.8)$$

Furthermore, ν is the kinematic viscosity, α is the thermal diffusivity of the fluid, g is the gravitational acceleration, β is the coefficient of thermal expansion, U and L_c are the characteristic velocity and length, respectively, T_w is the body/wall temperature, and T_0 is a reference temperature.

3 The direct-forcing immersed boundary projection method

In this section, we propose the direct-forcing IB projection method for simulating the heat transfer in the TFSI problem with a rigid solid body immersed in the fluid. First,

let us discretize the time variable of the system of Eqs. (2.4a)-(2.4i), with the spatial variable being left continuous. As for the spatial discretization, we use second-order centered differences over a staggered Cartesian grid that will be described later in Section 4. Considering the implicit second-order backward differentiation for discretizing the time variable, we obtain the following nonlinear boundary value problem at time $t = t_{n+1}$:

$$\frac{3\mathbf{u}^{n+1} - 4\mathbf{u}^n + \mathbf{u}^{n-1}}{2\Delta t} - P_1 \nabla^2 \mathbf{u}^{n+1} + [(\mathbf{u} \cdot \nabla) \mathbf{u}]^{n+1} + \nabla p^{n+1} - P_2 \theta^{n+1} \mathbf{e} = \mathbf{F}^{n+1} \quad \text{in } \Omega, \quad (3.1a)$$

$$\nabla \cdot \mathbf{u}^{n+1} = 0 \quad \text{in } \Omega, \quad (3.1b)$$

$$\mathbf{u}^{n+1} = \mathbf{u}_s^{n+1} \quad \text{in } \overline{\Omega}_s^{n+1}, \quad (3.1c)$$

$$\mathbf{u}^{n+1} = \mathbf{u}_b^{n+1} \quad \text{on } \partial\Omega, \quad (3.1d)$$

$$\frac{3\theta^{n+1} - 4\theta^n + \theta^{n-1}}{2\Delta t} - P_3 \nabla^2 \theta^{n+1} + \mathbf{u}^{n+1} \cdot \nabla \theta^{n+1} = E^{n+1} \quad \text{in } \Omega, \quad (3.1e)$$

$$\theta^{n+1} = \theta_b^{n+1} \quad \text{on } \partial\Omega, \quad (3.1f)$$

$$\theta^{n+1} = \theta_s^{n+1} \quad \text{on } \partial\Omega_s^{n+1} \quad \text{or} \quad -\kappa(\nabla \theta^{n+1} \cdot \mathbf{n}) = Q_s^{n+1} \quad \text{on } \partial\Omega_s^{n+1}, \quad (3.1g)$$

where the nonlinear convection term $[(\mathbf{u} \cdot \nabla) \mathbf{u}]^{n+1}$ and the velocity-temperature coupling term $\mathbf{u}^{n+1} \cdot \nabla \theta^{n+1}$ can be approximated by

$$[(\mathbf{u} \cdot \nabla) \mathbf{u}]^{n+1} = 2(\mathbf{u}^n \cdot \nabla) \mathbf{u}^n - (\mathbf{u}^{n-1} \cdot \nabla) \mathbf{u}^{n-1} + \mathcal{O}(\Delta t^2), \quad (3.2a)$$

$$\mathbf{u}^{n+1} \cdot \nabla \theta^{n+1} = \mathbf{u}^{n+1} \cdot \nabla (2\theta^n - \theta^{n-1}) + \mathcal{O}(\Delta t^2). \quad (3.2b)$$

It is highly inefficient in solving the boundary value problem (3.1a)-(3.1g) directly, even if \mathbf{F}^{n+1} and E^{n+1} are already known, because the algebraic system associated with space-discretization of the boundary value problem is rather large. This is the reason for proposing the fractional step approach to decouple the computations of \mathbf{u}^{n+1} , p^{n+1} , and θ^{n+1} .

In what follows, we introduce the direct-forcing IB approach combined with the Choi-Moin projection scheme [5]. The virtual force \mathbf{F}^{n+1} and virtual heat source E^{n+1} will be specified in the method when we decouple the time-discretized problem (3.1a)-(3.1g). The direct-forcing IB projection method can be divided into two parts, one approximating the incompressible viscous fluid for velocity \mathbf{u}^{n+1} , pressure p^{n+1} and virtual force \mathbf{F}^{n+1} , and the other one approximating the energy equation for temperature θ^{n+1} and virtual heat source E^{n+1} .

3.1 Solving the incompressible viscous fluid by the Choi-Moin scheme

Using a semi-implicit approximation combined with the Choi-Moin projection scheme, we decouple the nonlinear system (3.1a)-(3.1d) through the following three steps:

(S1) Solve for the intermediate velocity fields $\tilde{\mathbf{u}}$ and \mathbf{u}^* by considering

$$\frac{3\tilde{\mathbf{u}} - 4\mathbf{u}^n + \mathbf{u}^{n-1}}{2\Delta t} - P_1 \nabla^2 \tilde{\mathbf{u}} + \mathcal{P}[(\mathbf{u} \cdot \nabla)\mathbf{u}]^{n+1} + \nabla p^n - P_2 \theta^n \mathbf{e} = \mathbf{F}^n \quad \text{in } \Omega, \quad (3.3a)$$

$$\tilde{\mathbf{u}} = \mathbf{u}_b^{n+1} \quad \text{on } \partial\Omega, \quad (3.3b)$$

$$\frac{3\mathbf{u}^* - 3\tilde{\mathbf{u}}}{2\Delta t} - \nabla p^n = \mathbf{0} \quad \text{in } \Omega, \quad (3.3c)$$

where the term $\mathcal{P}[(\mathbf{u} \cdot \nabla)\mathbf{u}]^{n+1}$ in (3.3a) denotes the explicit second-order in time approximation to $[(\mathbf{u} \cdot \nabla)\mathbf{u}]^{n+1}$ given in (3.2a).

(S2) Determine the intermediate velocity \mathbf{u}^{**} and the pressure increment φ^{n+1} by solving

$$\frac{3\mathbf{u}^{**} - 3\mathbf{u}^*}{2\Delta t} + \nabla \varphi^{n+1} = \mathbf{0} \quad \text{in } \Omega, \quad (3.4a)$$

$$\nabla \cdot \mathbf{u}^{**} = 0 \quad \text{in } \Omega, \quad (3.4b)$$

$$\mathbf{u}^{**} \cdot \mathbf{n} = \mathbf{u}^* \cdot \mathbf{n} \quad \text{on } \partial\Omega. \quad (3.4c)$$

The unique solvability of the system (3.4a)-(3.4c) is ensured by the Helmholtz-Hodge decomposition [6]. Assume that the solution $(\mathbf{u}^{**}, \varphi^{n+1})$ is sufficiently smooth, then it is equivalent to solve the homogeneous Neumann problem of the pressure increment φ^{n+1}

$$\nabla^2 \varphi^{n+1} = \frac{3}{2\Delta t} \nabla \cdot \mathbf{u}^* \quad \text{in } \Omega, \quad (3.5a)$$

$$\nabla \varphi^{n+1} \cdot \mathbf{n} = 0 \quad \text{on } \partial\Omega, \quad (3.5b)$$

and then define the velocity field \mathbf{u}^{**} by

$$\mathbf{u}^{**} = \mathbf{u}^* - \frac{2\Delta t}{3} \nabla \varphi^{n+1} \quad \text{in } \Omega. \quad (3.6)$$

In practical computations, we additionally impose the condition $\int_{\Omega} \varphi^{n+1} dx = 0$ to the Neumann Poisson problem (3.5a)-(3.5b) for the uniqueness of solution. From (3.1a), (3.3a), (3.3c), (3.4a), and (3.5a), one can verify that the pressure should be defined as

$$p^{n+1} := \varphi^{n+1} - P_1 \nabla \cdot \tilde{\mathbf{u}} \quad \text{in } \Omega. \quad (3.7)$$

We will give some technical details on why we define p^{n+1} as (3.7) in the Appendix.

(S3) In order to make the velocity of solid body region to cope with prescribed solid body velocity \mathbf{u}_s^{n+1} , the increment of virtual force is given by

$$\delta \mathbf{F} := \eta \frac{3\mathbf{u}_s^{n+1} - 3\mathbf{u}^{**}}{2\Delta t} \quad \text{in } \Omega, \quad (3.8)$$

where the indicator function $\eta(t_{n+1}, \mathbf{x})$ is defined by

$$\eta(t_{n+1}, \mathbf{x}) = \begin{cases} 1, & \mathbf{x} \in \overline{\Omega}_s^{n+1}, \\ 0, & \mathbf{x} \notin \overline{\Omega}_s^{n+1}. \end{cases} \quad (3.9)$$

The technical detail on why we define δF as (3.8) is given in the Appendix. We then solve the velocity \mathbf{u}^{n+1} by directly setting

$$\frac{3\mathbf{u}^{n+1} - 3\mathbf{u}^{**}}{2\Delta t} = \delta F := \eta \frac{3\mathbf{u}_s^{n+1} - 3\mathbf{u}^{**}}{2\Delta t}. \quad (3.10)$$

In other words, in this step, we simply set

$$\mathbf{u}^{n+1} = \begin{cases} \mathbf{u}^{**} & \text{in } \overline{\Omega} \setminus \overline{\Omega}_s^{n+1}, \\ \mathbf{u}_s^{n+1} & \text{in } \overline{\Omega}_s^{n+1}. \end{cases} \quad (3.11)$$

Then the virtual force at time $t = t^{n+1}$ is defined as

$$\mathbf{F}^{n+1} := \mathbf{F}^n + \delta F = \mathbf{F}^n + \eta \frac{3\mathbf{u}_s^{n+1} - 3\mathbf{u}^{**}}{2\Delta t} \quad \text{in } \Omega. \quad (3.12)$$

Note that according to the indicator function η defined in (3.9), the virtual force \mathbf{F}^{n+1} is only distributed on the solid body region $\overline{\Omega}_s^{n+1}$.

3.2 Solving the energy equation for temperature

Once we obtain the velocity field \mathbf{u}^{n+1} , the boundary value problem (3.1e)-(3.1g) for heat equation can be approximated by splitting it into two steps:

(S4) Solve for the intermediate temperature θ^* with previous virtual heat source E^n :

$$\frac{3\theta^* - 4\theta^n + \theta^{n-1}}{2\Delta t} - P_3 \nabla^2 \theta^* + \mathbf{u}^{n+1} \cdot \nabla (2\theta^n - \theta^{n-1}) = E^n \quad \text{in } \Omega, \quad (3.13a)$$

$$\theta^* = \theta_b \quad \text{on } \partial\Omega. \quad (3.13b)$$

Here we replace the convection term $\mathbf{u}^{n+1} \cdot \nabla \theta^{n+1}$ in (3.1e) with the second-order in time approximation $\mathbf{u}^{n+1} \cdot \nabla (2\theta^n - \theta^{n-1})$; see (3.2b). This leads to an advantage that the matrices of the linear systems associated with the finite difference discretizations of the boundary value problem (3.13a)-(3.13b) are always same for all time steps.

(S5) In order to ensure the thermal boundary condition (3.1g) on the immersed solid boundary $\partial\Omega_s^{n+1}$, we first define the increment of the virtual heat source δE as

$$\delta E := \eta_\theta \frac{3\tilde{\theta}_s^{n+1} - 3\theta^*}{2\Delta t} \quad \text{in } \Omega, \quad (3.14)$$

where $\tilde{\theta}_s^{n+1} = \theta_s^{n+1}$ if we consider the Dirichlet boundary condition (2.2). Otherwise, if we consider the heat flux boundary condition (2.3), then $\tilde{\theta}_s^{n+1}$ will be specified later in the next subsection. Moreover, the indicator function η_θ is defined as

$$\eta_\theta(t_{n+1}, \mathbf{x}) = \begin{cases} 1, & \mathbf{x} \in \bar{\Omega}_s^{n+1} \text{ and near } \partial\Omega_s^{n+1}, \\ 0, & \text{otherwise.} \end{cases} \quad (3.15)$$

Then observing (3.1e) and (3.13a), we solve θ^{n+1} by directly setting

$$\frac{3\theta^{n+1} - 3\theta^*}{2\Delta t} = \delta E = \eta_\theta \frac{3\tilde{\theta}_s^{n+1} - 3\theta^*}{2\Delta t}. \quad (3.16)$$

That is, in this step, we simply set

$$\theta^{n+1} = \begin{cases} \tilde{\theta}_s^{n+1}, & \mathbf{x} \in \bar{\Omega}_s^{n+1} \text{ and near } \partial\Omega_s^{n+1}, \\ \theta^*, & \text{otherwise,} \end{cases} \quad (3.17)$$

and finally, the virtual heat source at time $t = t^{n+1}$ is defined as

$$E^{n+1} := E^n + \delta E = E^n + \eta_\theta \frac{3\tilde{\theta}_s^{n+1} - 3\theta^*}{2\Delta t} \text{ in } \Omega. \quad (3.18)$$

According to (3.14), the virtual heat source E^{n+1} is only located inside the solid region $\bar{\Omega}_s^{n+1}$ near the boundary $\partial\Omega_s^{n+1}$ for ensuring the thermal boundary condition (3.1g) on the boundary $\partial\Omega_s^{n+1}$.

3.3 Imposing the thermal boundary conditions on immersed solid boundary

To impose the Dirichlet thermal boundary condition (2.2) on the immersed solid boundary $\partial\Omega_s^{n+1}$, we can easily set $\tilde{\theta}_s^{n+1} = \theta_s^{n+1}$ in (3.14). On the other hand, for the Neumann thermal boundary condition (2.3), we first note that by Taylor's expansion,

$$\frac{\partial\theta^{n+1}}{\partial\mathbf{n}} \Big|_{\partial\Omega_s^{n+1}} = \frac{\tilde{\theta}_s^{n+1} - \hat{\theta}^*}{2d} + \mathcal{O}(d^2), \quad (3.19)$$

where $\tilde{\theta}_s^{n+1}$ is the temperature at the position $P(\tilde{\theta}_s^{n+1})$ indicated in Fig. 1, $\hat{\theta}^*$ is the temperature at the position $P(\hat{\theta}^*)$ that has distance $2d$ from $P(\tilde{\theta}_s^{n+1})$ along the normal direction to $\partial\Omega_s^{n+1}$, and d is the distance between $P(\tilde{\theta}_s^{n+1})$ and $\partial\Omega_s^{n+1}$, that is,

$$\text{dist}(P(\tilde{\theta}_s^{n+1}), \partial\Omega_s^{n+1}) = d = \text{dist}(P(\hat{\theta}^*), \partial\Omega_s^{n+1}). \quad (3.20)$$

Therefore, from (2.3), we obtain an accurate approximation of $\tilde{\theta}_s^{n+1}$ by rearranging (3.19),

$$\tilde{\theta}_s^{n+1} = \hat{\theta}^* + 2d \frac{\partial\theta^{n+1}}{\partial\mathbf{n}} \Big|_{\partial\Omega_s^{n+1}} + \mathcal{O}(d^3) = \hat{\theta}^* - \frac{2d}{\kappa} Q_s + \mathcal{O}(d^3). \quad (3.21)$$

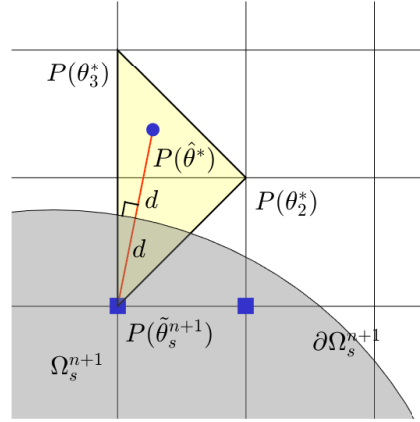


Figure 1: A schematic diagram of the interpolation scheme for the Neumann thermal boundary condition on the immersed solid boundary $\partial\Omega_s^{n+1}$.

The temperature $\hat{\theta}^*$ can be computed by using the piecewise linear interpolation,

$$\hat{\theta}^* = \tilde{\theta}_s^{n+1} \phi_1(P(\hat{\theta}^*)) + \theta_2^* \phi_2(P(\hat{\theta}^*)) + \theta_3^* \phi_3(P(\hat{\theta}^*)) + \mathcal{O}(d^2), \quad (3.22)$$

where $\phi_k, k=1,2,3$, are the usual linear finite element basis that are defined on the triangle determined by the three vertices $P(\tilde{\theta}_s^{n+1})$, $P(\theta_2^*)$, and $P(\theta_3^*)$. Finally, substituting (3.22) into (3.21), we obtain an $\mathcal{O}(d^2)$ -approximation to $\tilde{\theta}_s^{n+1}$, which will be used in (3.14),

$$\tilde{\theta}_s^{n+1} \approx \frac{\theta_2^* \phi_2(P(\hat{\theta}^*)) + \theta_3^* \phi_3(P(\hat{\theta}^*)) - \frac{2d}{\kappa} Q_s}{1 - \phi_1(P(\hat{\theta}^*))}. \quad (3.23)$$

We conclude this section with several remarks.

Remark 3.1. The direct-forcing IB projection method described in this section can easily be modified as an iterative scheme, if necessary. For example, once we obtain pressure p^{n+1} from (3.7), temperature θ^{n+1} from (3.17), virtual force F^{n+1} from (3.12), and virtual heat source E^{n+1} from (3.18), we can replace p^n , θ^n and F^n in (3.3a) with p^{n+1} , θ^{n+1} and F^{n+1} , respectively, and replace E^n in (3.13a) with E^{n+1} to form an iterative scheme.

Remark 3.2. Consider the case that the immersed solid $\bar{\Omega}_s$ is not stationary, i.e., $u_s \neq 0$. Since the virtual fluid force F^{n+1} in (3.1a) is distributed only on the solid region $\bar{\Omega}_s^{n+1}$, the position of the solid region will be misregistered if we use F^n , which is distributed only on $\bar{\Omega}_s^n$, to approximate F^{n+1} . As a result, it may lose accuracy and stability unless the time step Δt is sufficiently small. In such a case, we can modify the proposed direct-forcing method by simply setting the right-hand side of (3.3a) to be zero (i.e., F^n is replaced

by $\mathbf{0}$) and then directly define $F^{n+1} := \eta(3\mathbf{u}_s^{n+1} - 3\mathbf{u}^{**})/(2\Delta t)$ in (3.12). With the same idea, we set the right-hand side of (3.13a) to be zero and then directly define $E^{n+1} := \eta_\theta(3\tilde{\theta}_s^{n+1} - 3\theta^*)/(2\Delta t)$ in (3.18). We remark that a similar idea can be found in [16, 27], where the authors studied the FSI problems without a thermal effect.

Remark 3.3. It has been pointed out in [14] that the direct-forcing IB projection method proposed in [16, 17, 27] for the FSI problems is not always convergent when the direct-forcing approach combined with an arbitrarily chosen projection scheme unless the time step Δt is sufficiently small. That is because an inconsistency problem may arise in the method. It has also been indicated that the Choi-Moin projection scheme is an appropriate operator splitting scheme to alleviate the inconsistency. Moreover, a two-stage prediction-correction procedure has been proposed in [14] that can reduce the inconsistency as well. However, in the present paper, we use the previous virtual force F^n and virtual heat source E^n as the predictors instead of the two-stage approach; see both first steps in Section 3.1 and Section 3.2.

Remark 3.4. It has been pointed out from the numerical results of the problem of flow over cylinder reported in [14], we can find that the divergence-free condition of the direct-forcing IB projection approach is generally satisfied except only at the leading edge of the cylinder. Observing into more carefully, these non-zero divergence spots appear as pairs of mass sink and source of equal magnitude (doublet), which upholds global mass conservation of the direct-forcing IB projection method.

4 Numerical experiments

In this section, we perform numerical simulations of several TFSI problems to validate the newly proposed method's efficiency and reliability. The heat transfer examples under consideration include the natural heat convection in a square enclosure with a heated cylinder, the natural heat convection in an annulus, the forced heat convection without buoyancy over a cylinder with constant heat flux, and the mixed heat convection with buoyancy in the lid-driven cavity with an embedded cylinder. In these examples, the immersed solid bodies are all stationary $\mathbf{u}_s \equiv \mathbf{0}$, except in Example 4.3, in which we also consider the fluid flow over a periodically oscillating heated solid. We apply the second-order centered differences over a staggered Cartesian grid for the space-discretizations in the solution procedure, where the unknown functions, u and F_1 , v and F_2 , p and θ and E , are respectively approximated at the points marked by \rightarrow , \uparrow and \bullet ; see Fig. 2. Moreover, for the static solid body problems, we assume that the numerical simulation reaches a steady-state by setting the following convergence criterion for all unknown functions:

$$\frac{\|q^{n+1} - q^n\|_1}{\|q^{n+1}\|_1} < 10^{-5}. \quad (4.1)$$

From the numerical results presented below, we can find that all these examples show the high capability of the proposed method in simulating heat transfer phenomena in

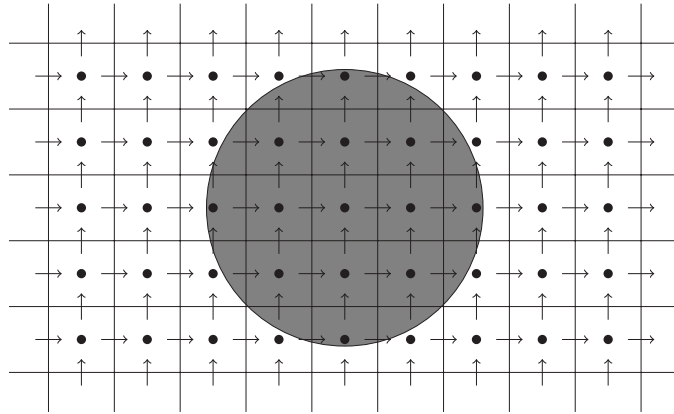


Figure 2: A schematic diagram of the computational domain Ω , where the unknown functions, u and F_1 , v and F_2 , p and θ and E , are approximated at the points marked by \rightarrow , \uparrow and \bullet , respectively.

the complex-geometry TFSI problems. We can also see that our results are in excellent agreement with the previous works in the literature.

Example 4.1 (Natural heat convection in a square enclosure with a heated cylinder). In this example, we study the natural heat convection in a square enclosure with a heated cylinder to validate the proposed method. The computational domain is taken as $\Omega = (0,1) \times (0,1)$ enclosing a heated cylinder centered at $(0.5,0.5)$ with diameter $D = 0.2$. The Dirichlet boundary conditions of velocity and temperature are shown in Fig. 3. Our simulations are implemented on three large Rayleigh numbers, $Ra = 10^4, 10^5, 10^6$, all with a fixed Reynolds number $Re = 100$ and a fixed Prandtl number $Pr = 0.7$.

We consider a uniform Cartesian grid of Ω with the grid size $\Delta x = \Delta y = 1/128$. It

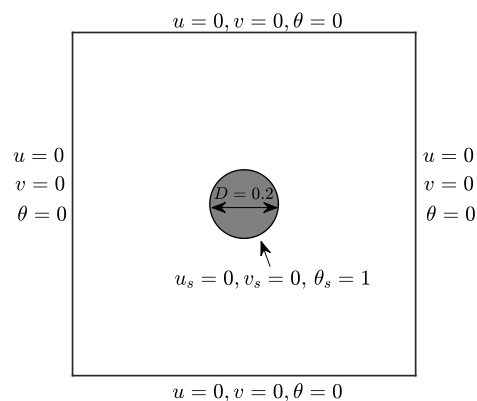


Figure 3: Example 4.1 Boundary conditions of the problem of natural heat convection in a square enclosure with a stationary heated cylinder.

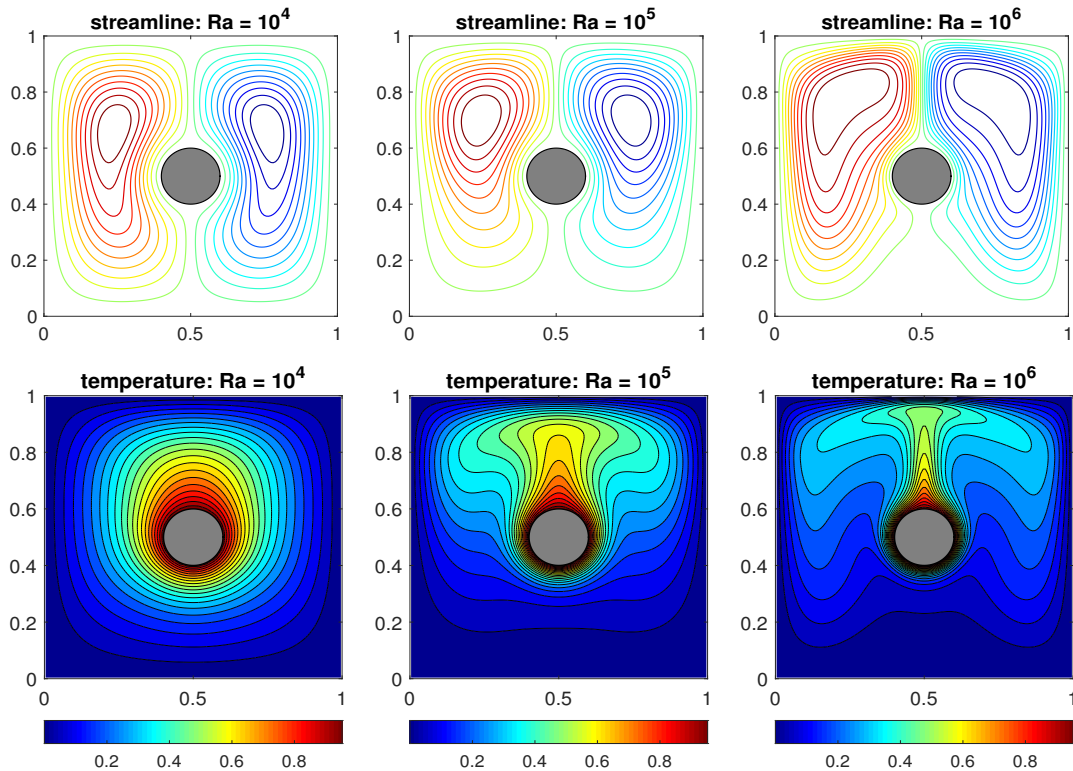


Figure 4: Streamlines (upper row) and isotherms (lower row with color bar) of the natural heat convection in a square enclosure with a stationary heated cylinder for different Rayleigh numbers $Ra = 10^4, 10^5, 10^6$.

has been observed in [3] that as the Rayleigh number Ra increasing, the heat transfer in the enclosure is mainly governed by natural convection and moreover, larger Ra can enhance the fast heat transfer process due to the larger term of the buoyancy $P_2\theta e$ in (2.4a), where $P_2 = RaPr$. Therefore, we take a small time step $\Delta t = 10^{-5}$ to accurately capture the heat transfer phenomena. The obtained numerical results of streamlines and isotherms are shown in Fig. 4. One can find that as the Rayleigh number Ra increases to 10^6 , the thermal plume strongly impinges on the top of the enclosure to form a thermal boundary layer and enhances the heat transfer. Our results are similar to those reported in [3].

Example 4.2 (Natural heat convection in an annulus). In this example, we consider the natural heat convection in an annulus [11, 37, 39] to validate the performance of the proposed method for dealing with the Neumann thermal boundary condition. We take a larger computational domain $\Omega = (0,5) \times (0,5)$ which encloses the annulus. It is interesting to note that two regions outside the annulus are both treated as stationary solid bodies. The setting of boundary conditions are shown in Fig. 5, where the annulus is

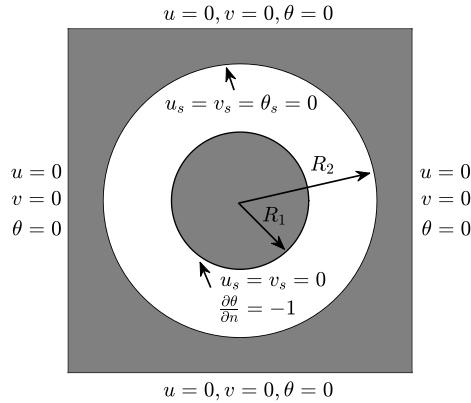


Figure 5: Example 4.2 Boundary conditions of the problem of natural heat convection in an annulus.

composed of an inner cylinder of radius $R_1 = 1$ and an outer cylinder of radius $R_2 = 2$ both centered at $(2.5, 2.5)$. A non-homogeneous Neumann thermal boundary condition $\partial\theta/\partial n = -1$ on the inner cylinder and a zero Dirichlet thermal boundary condition $\theta = 0$ on the outer cylinder are given. The zero boundary conditions of velocity and temperature are imposed elsewhere.

In our simulations, we first fix the Reynolds number $Re = 100$ and the Prandtl number $Pr = 0.7$, and then consider two different Rayleigh numbers, $Ra = 5700$ and $Ra = 50000$. We partition the domain Ω into a uniform Cartesian grid with $\Delta x = \Delta y = 1/128$ and the time step is chosen as $\Delta t = 10^{-4}$. Numerical results are depicted in Fig. 6, where the isotherms and streamlines of different Rayleigh numbers are shown. In order to compare the numerical results with those reported in [11, 37, 39], we define the dimensionless temperature Θ on the left-hand part of the inner cylinder surface as

$$\Theta := \frac{\theta - \theta_\infty}{Q_s(R_2 - R_1)/\kappa'} \tag{4.2}$$

where θ_∞ is the constant temperature of the outer cylinder. In this example, we have $\theta_\infty = 0$, $R_2 - R_1 = 1$, $Q_s = 1$, and $\kappa = 1$. Thus, $\Theta = \theta$. Note that for every point located at the left-hand part of the inner cylinder surface, it corresponds to a unique angle that is measured in the counterclockwise rotation from the uppermost point of the inner cylinder surface to that surface point with respect to the cylinder center $(2.5, 2.5)$. We plot the distribution of Θ in the angle variable in Fig. 7, from which we can find that the numerical results are in good agreement with those obtained in [11, 37, 39].

Next, we study the convergence behavior of the proposed method. We consider the Rayleigh number $Ra = 5700$ and different grid sizes, $h = 2^{-i}$ for $i = 4, 5, 6, 7, 8$. The time step is still taken as $\Delta t = 10^{-4}$. Since there is no exact solution for this example, we use numerical results obtained by the present method at the finest grid size $h = 2^{-9} = 1/512$ as the reference solution. The numerical results are reported in Table 1. We can find from

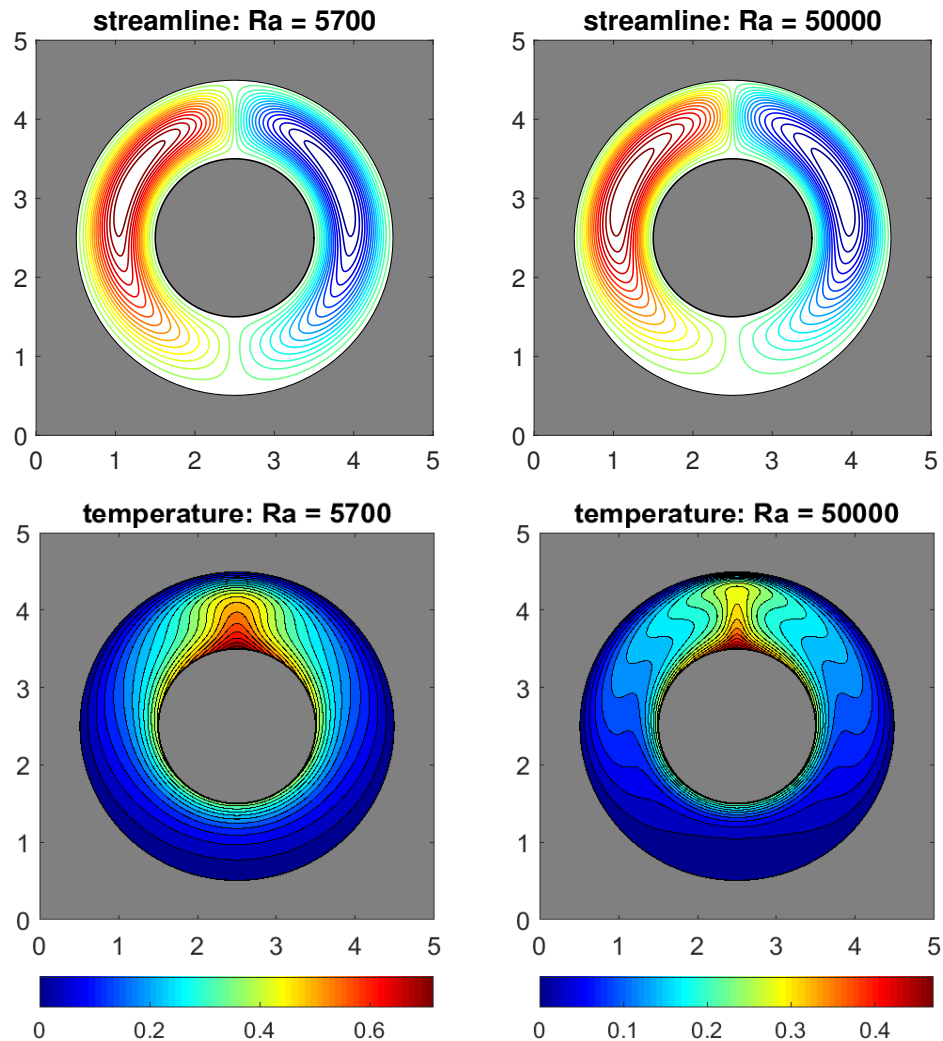


Figure 6: Streamlines (upper row) and isotherms (lower row with color bar) of the natural heat convection in an annulus for Rayleigh numbers $Ra = 5700, 50000$.

Table 1 that the spatial convergence rates of all unknowns seem to be super-linear in the 1-norm and 2-norm while less than linear in the maximum norm.

Example 4.3 (Forced heat convection without buoyancy over a stationary cylinder). In this example, we consider the forced heat convection without buoyancy over a stationary cylinder with a constant heat flux [1, 2, 11, 32, 37]. A circular cylinder Ω_s of diameter $D = 1$ centered at $(0,0)$ is contained in a sufficiently large computational domain $\Omega = (-14D, 20D) \times (-15D, 15D)$. On the surface of the cylinder $\partial\Omega_s$, a non-homogeneous

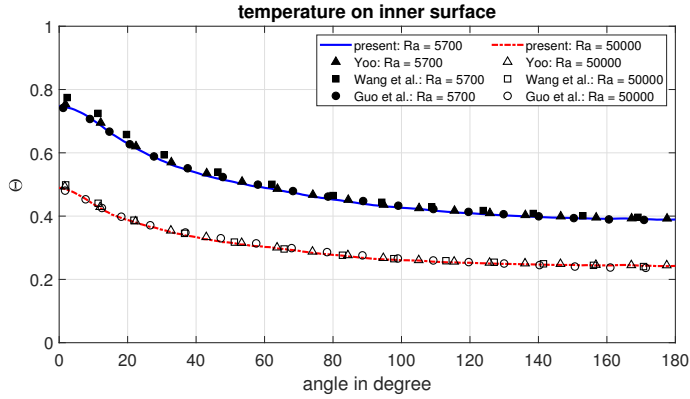


Figure 7: Comparison of the local temperature distribution on the inner cylinder surface of the proposed method and the methods of Guo et al. [11], Wang et al. [37], and Yoo [39] for Rayleigh numbers $Ra=5700, 50000$.

Neumann thermal boundary condition $\partial\theta/\partial n = -1$ and the no-slip velocity boundary condition are imposed. The detailed boundary conditions are depicted in Fig. 8.

In the simulations, we consider three different Reynolds numbers, $Re=10, 20, 40$, with a fixed Prandtl number $Pr=0.7$. We use a uniform Cartesian grid with $\Delta x = \Delta y = 1/100$

Table 1: Error behavior of the numerical solutions of Example 4.2 with $Ra=5700$.

	$1/h$	1-norm	order	2-norm	order	max-norm	order
u_h	16	2.5236e-1	—	1.3103e-1	—	3.1572e-1	—
	32	9.9273e-2	1.35	5.4103e-2	1.28	1.7847e-1	0.82
	64	4.2363e-2	1.23	2.5824e-2	1.07	1.1036e-1	0.69
	128	1.9976e-2	1.08	1.2724e-2	1.02	7.3368e-2	0.59
	256	9.4106e-3	1.09	5.8283e-3	1.13	4.7045e-2	0.64
v_h	16	3.4501e-1	—	1.9544e-1	—	4.7039e-1	—
	32	1.2457e-1	1.47	7.5175e-2	1.38	2.6664e-1	0.82
	64	5.4941e-2	1.18	3.6056e-2	1.06	1.7073e-1	0.64
	128	2.6128e-2	1.07	1.7694e-2	1.03	1.1441e-1	0.58
	256	1.2079e-2	1.11	8.0559e-3	1.14	7.2362e-2	0.66
p_h	16	5.1399e-1	—	1.1965e-1	—	9.8353e-1	—
	32	2.7099e-1	0.92	6.1402e-2	0.96	5.7592e-1	0.77
	64	6.5686e-2	2.04	1.4959e-2	2.04	3.7714e-1	0.61
	128	2.9742e-2	1.14	6.1096e-3	1.29	2.8193e-1	0.42
	256	1.5294e-2	0.96	3.0405e-3	1.01	2.1276e-1	0.41
θ_h	16	2.1610e-1	—	9.2559e-2	—	7.5566e-2	—
	32	9.7645e-2	1.15	4.2021e-2	1.14	4.0568e-2	0.90
	64	4.0106e-2	1.28	1.8536e-2	1.18	2.4017e-2	0.76
	128	1.6945e-2	1.24	8.2950e-3	1.16	1.4800e-2	0.70
	256	7.8559e-3	1.11	3.8893e-3	1.09	9.6077e-3	0.62

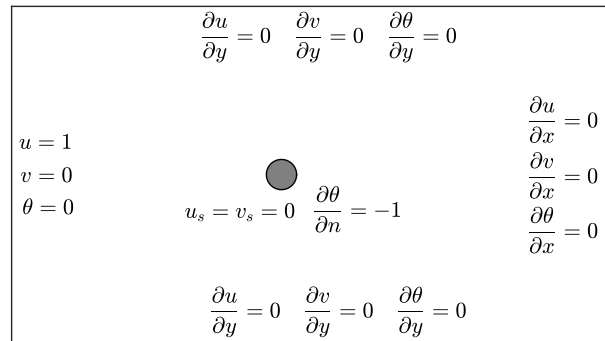


Figure 8: Example 4.3 Boundary conditions of the problem of forced heat convection without buoyancy over a stationary cylinder.

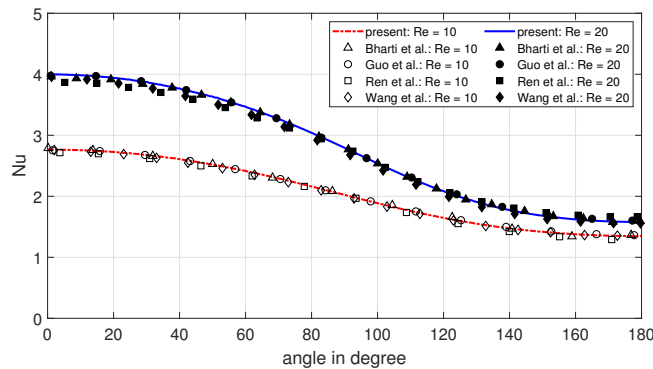


Figure 9: Comparison of the local Nusselt numbers Nu on the upper-half surface of the cylinder of the proposed method and the methods of Bharti et al. [2], Guo et al. [11], Ren et al. [32], and Wang et al. [37] for Reynolds numbers $Re = 10, 20$.

to discretize the computational domain Ω and take the time step $\Delta t = 10^{-3}$ for the time-discretization. For the sake of comparison with other numerical methods, we define the local Nusselt number $Nu(x)$ at point x of the cylinder surface, and the average Nusselt number \bar{Nu} on the whole surface as

$$Nu(x) := \frac{Q_s D}{\kappa(\theta(x) - \theta_\infty)} \quad \text{and} \quad \bar{Nu} := \frac{1}{\pi D} \int_{\partial\Omega_s} Nu(x) ds, \quad (4.3)$$

where the reference temperature is $\theta_\infty = 0$. In Fig. 9, we show the numerical results of local Nusselt numbers on the cylinder's upper-half surface. The results are compared with the previous studies, where the angle in degree is measured from the left endpoint of the upper-half surface to the right endpoint in a clockwise rotation with respect to the cylinder center $(0,0)$. Furthermore, a comparison of the average Nusselt numbers is also presented in Table 2. The results produced by the proposed method agree very well with those results reported in [1, 2, 11, 32, 37]. The streamlines and isotherms for different

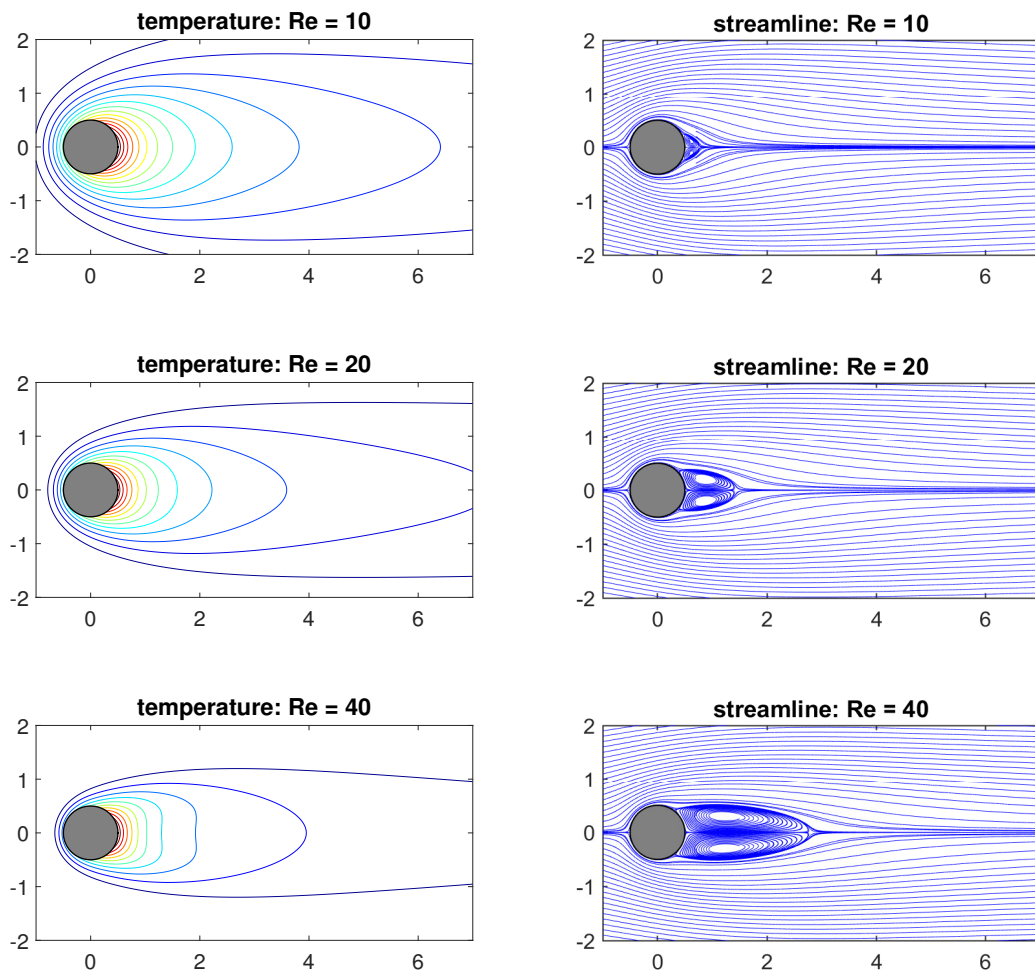


Figure 10: Isotherms (left column) and streamline (right column) near the cylinder for three different Reynolds numbers $Re = 10, 20, 40$.

Reynolds numbers are shown in Fig. 10.

Next, we perform the numerical experiments for higher Reynolds numbers on the time interval $[0, 200]$. We find that as the Reynolds number Re is sufficiently large, the symmetry of cylinder wake will be broken down, and the two vortices will be shed alternatively. Due to the influence of the velocity field, the temperature shows a similar shedding pattern. Fig. 11 shows the isotherms and vorticity contours for $Re = 200$ at time $T = 200$, where the vortex street shedding has been successfully revealed. In Fig. 12, we plot the time-average local Nusselt numbers on the cylinder's upper-half surface on time

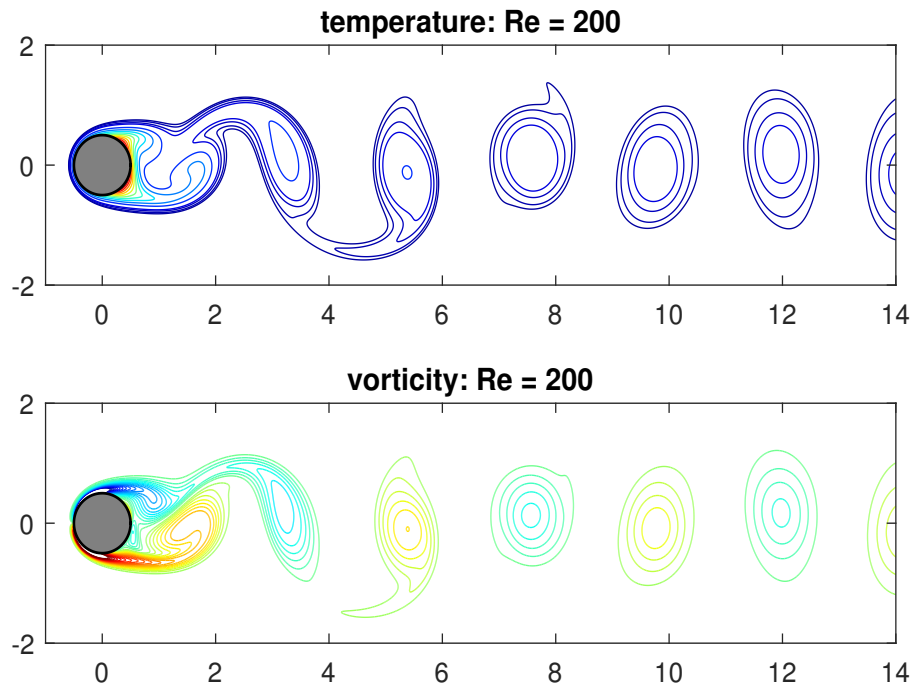


Figure 11: Isotherms and vorticity contours near the cylinder for Reynolds number $Re=200$ at time $T=200$.

interval $[0,200]$. One can see that the newly proposed method’s numerical results are similar to those obtained in [11, 13, 41].

We now consider the fluid flow over a periodically oscillating heated cylinder. That is, we have $\mathbf{u}_s \neq \mathbf{0}$. The problem setting is the same as the stationary case, except that on the surface of the cylinder $\partial\Omega_s$, a non-homogeneous Dirichlet thermal boundary condition $\theta=1$ is imposed. The center $(x_c(t), y_c(t))$ of the cylinder is vertically oscillating governed by the equation,

$$(x_c(t), y_c(t)) = (0, A \sin(2\pi ft)), \quad t \geq 0, \tag{4.4}$$

where $A=1$ and $f=0.2$ are the amplitude and frequency of the periodic oscillation, re-

Table 2: Comparison of the average Nusselt numbers of Example 4.3.

Methods	$Re=10$	$Re=20$	$Re=40$
Ahmad & Qureshi [1]	2.041	2.662	3.472
Bharti et al. [2]	2.0400	2.7788	3.7755
Guo et al. [11]	2.0466	2.7858	3.7856
Ren et al. [32]	2.0265	2.7413	3.7407
Wang et al. [37]	2.01	2.69	3.68
Present method	2.0400	2.7812	3.7846

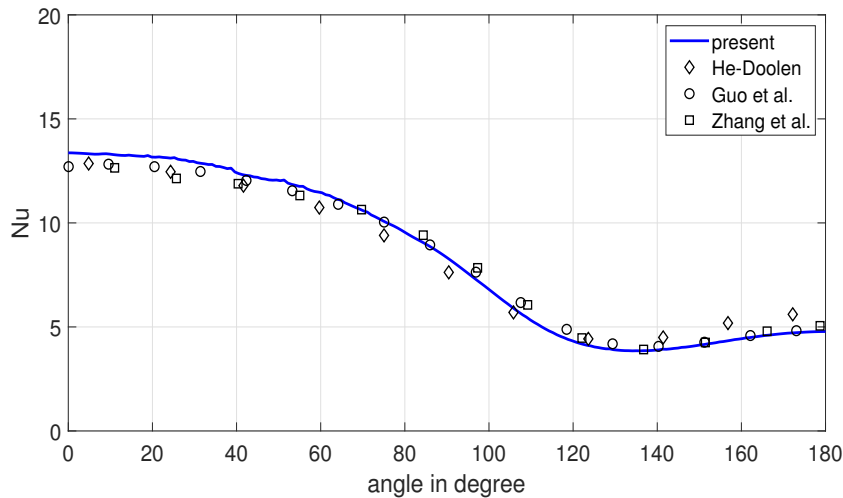


Figure 12: Comparison of the time-average local Nusselt numbers Nu on the upper-half surface of the cylinder on time interval $[0,200]$ of the proposed method and the methods of Guo et al. [11], He-Doolen [13], and Zhang et al. [41] for Reynolds number $Re = 200$.

spectively, and hence the period of the oscillation is $\mathbb{T} = 5$. Since the heated cylinder immersed in the fluid is periodically oscillating, in this example, we employ a slightly modified direct-forcing method described in Remark 3.2. Numerical results of the temperature and vorticity distributions near the cylinder for $Re = 200$ at different times $t = 45$ and $45 + \mathbb{T}/4$, $45 + 2\mathbb{T}/4$, $45 + 3\mathbb{T}/4$, and $45 + \mathbb{T}$ are displayed in Fig. 13. We can observe from Fig. 13 that the temperature and vorticity distributions show a similar periodic shedding pattern. Thus, the proposed method seems rather robust for simulating the TFSI problems with moving solid bodies immersed in the fluid.

Example 4.4 (Mixed heat convection with buoyancy in the lid-driven cavity with an embedded cylinder). This example is taken from [19] where a body-fitted approach based on the finite element formulation is used for the simulations. We consider the mixed heat convection with buoyancy in the lid-driven cavity $\Omega = (0,1) \times (0,1)$ with an embedded cylinder, where the cylinder is centered at $(0.5,0.5)$ with diameter $D = 0.4$. In this example, we will consider the homogeneous Neumann thermal boundary condition, i.e., the adiabatic boundary condition, on the immersed solid boundary. The detailed boundary conditions of velocity and temperature are displayed in Fig. 14.

Our simulations are implemented on four different Richardson numbers, $P_2 = Ri := Gr/Re^2 = 0.01, 1, 5, 10$, with a fixed Reynolds number $Re = 100$ and a fixed Prandtl number $Pr = 0.7$. The numerical computations are performed on a uniform Cartesian grid with $\Delta x = \Delta y = 1/250$ and the time step is taken as $\Delta t = 10^{-3}$. Note that in this example, the heat buoyancy effect $P_2\theta e$ in (2.4a) is relatively small. The isotherms and streamlines for different Richardson numbers are respectively depicted in Fig. 15 and Fig. 16. In Fig. 17,

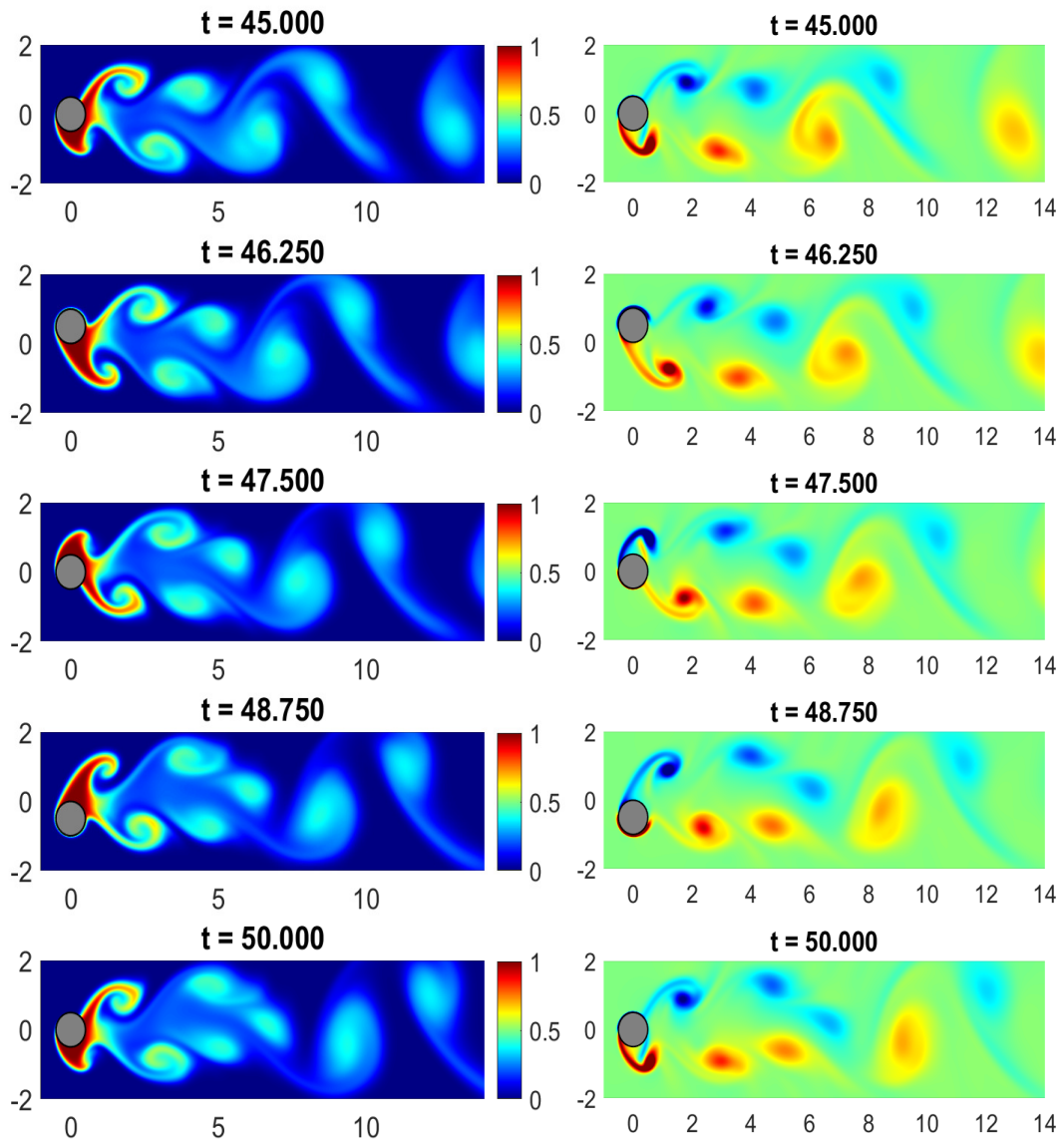


Figure 13: Temperature (left column) and vorticity (right column) distributions near the heated cylinder for $Re=200$ at different times $t=45$ and $45+\mathbb{T}/4$, $2\mathbb{T}/4$, $3\mathbb{T}/4$, \mathbb{T} , where $\mathbb{T}=5$.

we show the variation of temperature along a vertical line $x=0.15$ and a horizontal line $y=0.15$. These results are also compared with the previous study [19]. We find that our numerical results are in very good agreement with those presented in [19]. Moreover, in Fig. 18, we show the local Nusselt number Nu measured along the heated bottom wall,

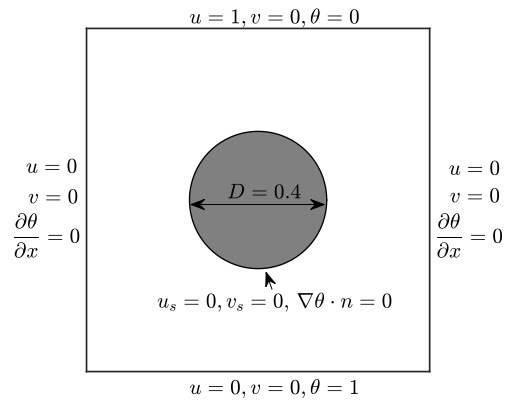


Figure 14: Example 4.4 Boundary conditions of the problem of mixed heat convection with buoyancy in the lid-driven cavity ow with an embedded cylinder.

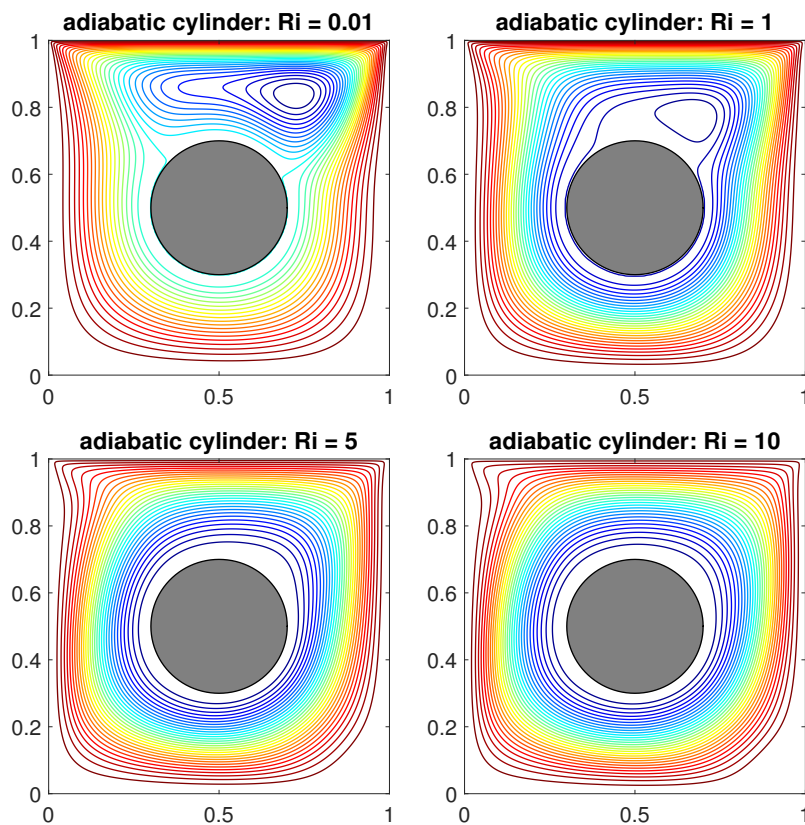


Figure 15: Streamlines of the mixed convection heat transfer in the lid-driven cavity flow with an embedded cylinder and homogeneous Neumann thermal boundary condition for different Richardson numbers, $Ri = 0.01, 1, 5, 10$.

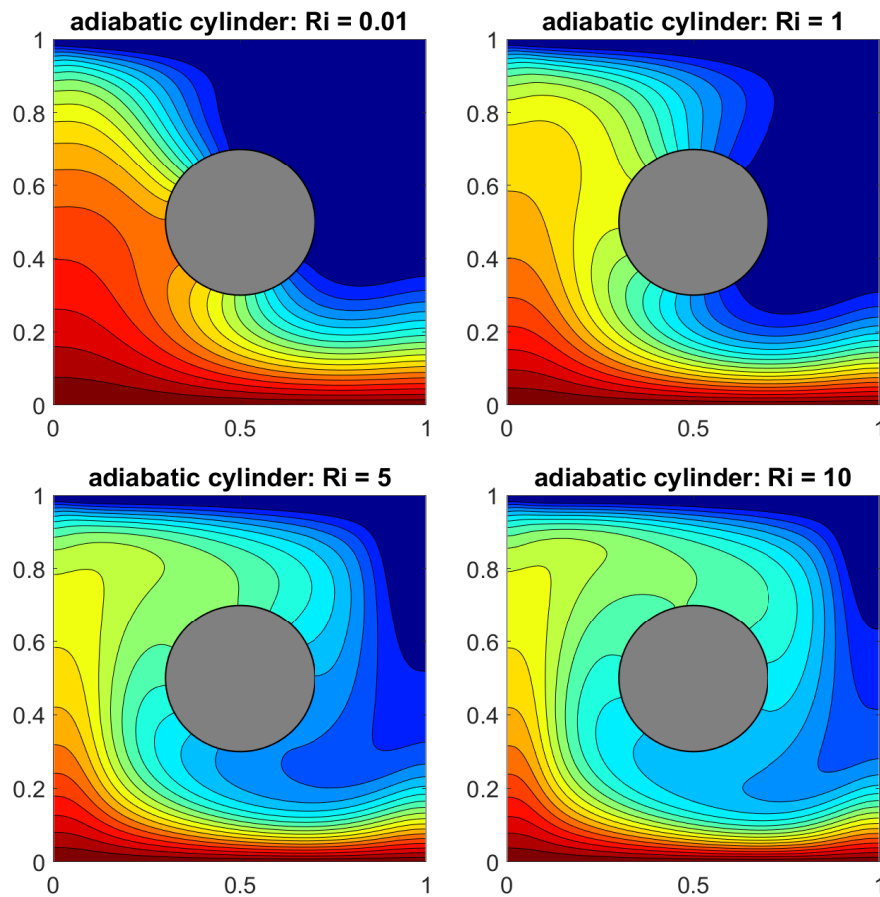


Figure 16: Isotherms of the mixed convection heat transfer in the lid-driven cavity flow with an embedded cylinder and homogeneous Neumann thermal boundary condition for different Richardson numbers, $Ri = 0.01, 1, 5, 10$.

defined as

$$Nu(x) := -\frac{\partial \theta}{\partial y}(x) \quad \text{for } x = (x, 0), \quad 0 \leq x \leq 1. \quad (4.5)$$

Again, the numerical results agree very well with those available in [19,37].

5 Summary and conclusions

The investigation of thermal fluid-structure interactions is of great importance in many applications of sciences and engineering. In this paper, we have developed an efficient direct-forcing IB projection method for analyzing heat transfer in the TFSI problems with a rigid solid immersed in the fluid. The proposed method is not only conceptually simple

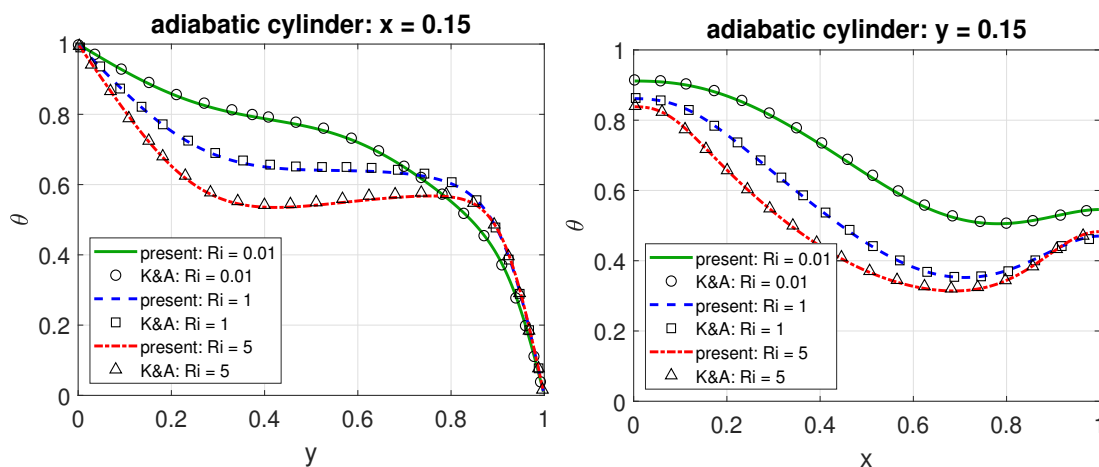


Figure 17: Comparison of the variation of temperature along a vertical line $x=0.15$ (left) and a horizontal line $y=0.15$ (right) of the proposed method and the method of Khanafer-Aithal [19] for different Richardson numbers, $Ri=0.01,1,5$.

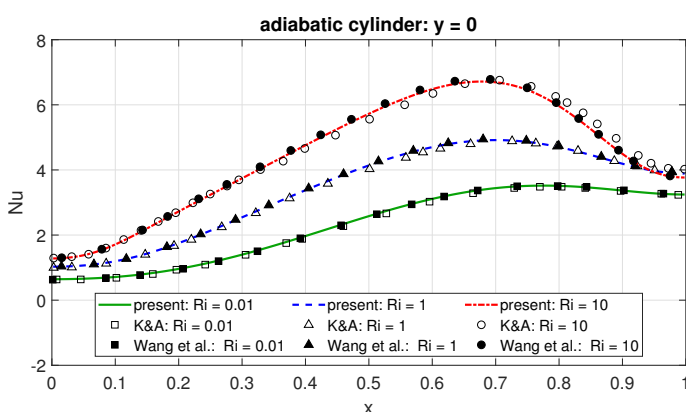


Figure 18: Comparison of the local Nusselt numbers Nu along the heated bottom wall $y=0$ of the proposed method and the methods of Khanafer-Aithal [19] and Wang et al. [37] for different Richardson numbers, $Ri=0.01,1,10$.

but also easy to implement. At first, the immersed solid body was regarded as made of fluid. Then a virtual force distributed only in the solid region was appended to the momentum equation as a forcing term to make the region behave like a real solid body and exactly satisfy the prescribed velocity, without using any Dirac delta functions that are necessary for the traditional IB methods. And a virtual heat source term, located inside the solid region near the boundary, was applied to the energy transport equation. It helps impose either the temperature (Dirichlet) or the heat flux (Neumann) boundary conditions on the immersed solid boundary.

After introducing the virtual force and virtual heat source, we have taken the implicit

second-order backward differentiation to discretize the time variable and applied the Choi-Moin projection scheme to split the nonlinear coupled system. As for spatial discretization, we have employed second-order centered differences over a staggered Cartesian grid to discretize the space variable on the entire domain, including the solid body region. Moreover, to tackle the most challenging case of imposing Neumann thermal boundary condition on the immersed solid boundary, we have devised a simple and accurate spatial approximation to incorporate the Neumann boundary condition into the proposed method. An exciting feature of this approach is that the virtual force and virtual heat source can be explicitly determined in the solution procedure. We have performed numerical experiments of several TFSI problems to verify the proposed direct-forcing IB projection method's simplicity and capability. Convergence tests show that the spatial convergence rates of all unknowns seem to be super-linear in the 1-norm and 2-norm while less than linear in the maximum norm.

We remark that the direct-forcing IB projection method for conjugate heat transfer [7, 26] in the TFSI problems deserves further investigation, although we did not study in this paper yet. Note that a similar idea proposed in this paper can be slightly modified to adapt to the TFSI problems with an immersed solid body governed by some motion equations. Moreover, a similar approach can also be applied to simulate the dynamics of the heat transfer process of FSI problems in the magnetohydrodynamic flow. All these issues deserve more consideration and discussion.

Appendix: the technical details of (3.7) and (3.8)

This Appendix section gives technical details on why we define p^{n+1} as (3.7) and δF as (3.8). First, adding Eqs. (3.3a) and (3.3c) gives

$$\frac{3\mathbf{u}^* - 4\mathbf{u}^n + \mathbf{u}^{n-1}}{2\Delta t} - P_1 \nabla^2 \tilde{\mathbf{u}} + \mathcal{P}[(\mathbf{u} \cdot \nabla) \mathbf{u}]^{n+1} - P_2 \theta^n \mathbf{e} = \mathbf{F}^n. \quad (\text{A.1})$$

Rewriting (3.3c) as

$$\tilde{\mathbf{u}} = \mathbf{u}^* - \frac{2\Delta t}{3} \nabla p^n, \quad (\text{A.2})$$

and then substituting (A.2) into (A.1), we get

$$\frac{3\mathbf{u}^* - 4\mathbf{u}^n + \mathbf{u}^{n-1}}{2\Delta t} - P_1 \nabla^2 \mathbf{u}^* + \mathcal{P}[(\mathbf{u} \cdot \nabla) \mathbf{u}]^{n+1} + \Delta \left(P_1 \frac{2\Delta t}{3} \nabla p^n \right) - P_2 \theta^n \mathbf{e} = \mathbf{F}^n. \quad (\text{A.3})$$

Adding Eqs. (A.3) and (3.4a) leads to

$$\begin{aligned} & \frac{3\mathbf{u}^{**} - 4\mathbf{u}^n + \mathbf{u}^{n-1}}{2\Delta t} - P_1 \nabla^2 \mathbf{u}^* + \mathcal{P}[(\mathbf{u} \cdot \nabla) \mathbf{u}]^{n+1} \\ & + \nabla \left(P_1 \frac{2\Delta t}{3} \Delta p^n + \varphi^{n+1} \right) - P_2 \theta^n \mathbf{e} = \mathbf{F}^n, \end{aligned} \quad (\text{A.4})$$

where we employ the identity $\Delta(\nabla p^n) = \nabla(\Delta p^n)$ provided p^n is sufficiently smooth. Reformulating (3.3c) as

$$\mathbf{u}^* = \mathbf{u}^{**} + \frac{2\Delta t}{3} \nabla \varphi^{n+1}, \quad (\text{A.5})$$

and substituting (A.5) into (A.4), we obtain

$$\begin{aligned} & \frac{3\mathbf{u}^{**} - 4\mathbf{u}^n + \mathbf{u}^{n-1}}{2\Delta t} - P_1 \nabla^2 \mathbf{u}^{**} + \mathcal{P}[(\mathbf{u} \cdot \nabla) \mathbf{u}]^{n+1} \\ & + \nabla \left(P_1 \frac{2\Delta t}{3} \Delta(p^n - \varphi^{n+1}) + \varphi^{n+1} \right) - P_2 \theta^n \mathbf{e} = \mathbf{F}^n. \end{aligned} \quad (\text{A.6})$$

Observing (3.1a) and (A.6), it is reasonable to define p^{n+1} by

$$p^{n+1} := P_1 \frac{2\Delta t}{3} \Delta(p^n - \varphi^{n+1}) + \varphi^{n+1}. \quad (\text{A.7})$$

From (3.3c) and (3.5a), we have

$$\frac{2\Delta t}{3} \Delta p^n = \nabla \cdot \mathbf{u}^* - \nabla \cdot \tilde{\mathbf{u}} \quad \text{and} \quad \frac{2\Delta t}{3} \Delta \varphi^{n+1} = \nabla \cdot \mathbf{u}^*, \quad (\text{A.8})$$

which combining with (A.7) implies (3.7), that is,

$$p^{n+1} := \varphi^{n+1} - P_1 \nabla \cdot \tilde{\mathbf{u}}. \quad (\text{A.9})$$

Next, let the increment of virtual force δF be defined as that in (3.8), that is,

$$\delta F := \eta \frac{3\mathbf{u}_s^{n+1} - 3\mathbf{u}^{**}}{2\Delta t}. \quad (\text{A.10})$$

Adding (3.10) to (A.6) and combining with (3.12), we obtain

$$\begin{aligned} & \frac{3\mathbf{u}^{n+1} - 4\mathbf{u}^n + \mathbf{u}^{n-1}}{2\Delta t} - P_1 \nabla^2 \mathbf{u}^{**} + \mathcal{P}[(\mathbf{u} \cdot \nabla) \mathbf{u}]^{n+1} \\ & + \nabla p^{n+1} - P_2 \theta^n \mathbf{e} = \mathbf{F}^n + \delta F =: \mathbf{F}^{n+1}. \end{aligned} \quad (\text{A.11})$$

Finally, by (3.11), we can conclude that (A.11) is a reasonable approximation to (3.1a).

Acknowledgements

The authors would like to thank the anonymous referees for their valuable comments and suggestions that substantially improved the original manuscript. This work was partially supported by the Ministry of Science and Technology of Taiwan under grants MOST 107-2115-M-035-007-MY2 (C.-S. You), MOST 106-2115-M-005-005-MY2 (P.-W. Hsieh), and MOST 106-2115-M-008-014-MY2 (S.-Y. Yang). The research of S.-Y. Yang was also partially supported by the National Center for Theoretical Sciences (NCTS), Taiwan.

References

- [1] R. A. AHMAD AND Z. H. QURESHI, *Laminar mixed convection from a uniform heat flux horizontal cylinder in a crossflow*, J. Thermophys. Heat Transfer, 6 (1992), pp. 277–287.
- [2] R. P. BHARTI, R. P. CHHABRA, AND V. ESWARAN, *A numerical study of the steady forced convection heat transfer from an unconfined circular cylinder*, Heat Mass Transfer, 43 (2007), pp. 639–648.
- [3] M.-J. CHERN, D. Z. NOOR, C.-B. LIAO, AND T.-L. HORNG, *Direct-forcing immersed boundary method for mixed heat transfer*, Commun. Comput. Phys., 18 (2015), pp.1072-1094.
- [4] P. H. CHIU, R. K. LIN, AND T. W. H. SHEU, *A differentially interpolated direct forcing immersed boundary method for predicting incompressible Navier-Stokes equations in time-varying complex geometries*, J. Comput. Phys., 229 (2010), pp. 4476–4500.
- [5] H. CHOI AND P. MOIN, *Effects of the computational time step on numerical solutions of turbulent flow*, J. Comput. Phys., 113 (1994), pp. 1-4.
- [6] A. J. CHORIN AND J. E. MARSDEN, *A Mathematical Introduction to Fluid Mechanics*, 2nd Edition, Springer-Verlag, New York, 1990.
- [7] S. DAS, A. PANDA, N. G. DEEN, AND J. A. M. KUIPERS, *A sharp-interface immersed boundary method to simulate convective and conjugate heat transfer through highly complex periodic porous structures*, Chem. Eng. Sci., 191 (2018), pp. 1–18.
- [8] F. DOMENICHINI, *On the consistency of the direct forcing method in the fractional step solution of the Navier-Stokes equations*, J. Comput. Phys., 227 (2008), pp. 6372–6384.
- [9] E. A. FADLUN, R. VERZICCO, P. ORLANDI, AND J. MOHD-YUSOF, *Combined immersed-boundary finite-difference methods for three-dimensional complex flow simulations*, J. Comput. Phys., 161 (2000), pp. 35–60.
- [10] J. L. GUERMOND, P. MINEV, AND J. SHEN, *An overview of projection methods for incompressible flows*, Comput. Methods Appl. Mech. Eng., 195 (2006), pp. 6011–6045.
- [11] T. GUO, E. SHEN, Z. LU, Y. WANG, AND L. DONG, *Implicit heat flux correction-based immersed boundary-finite volume method for thermal flows with Neumann boundary conditions*, J. Comput. Phys., 386 (2019), pp. 64–83.
- [12] R. D. GUY AND D. A. HARTENSTINE, *On the accuracy of direct forcing immersed boundary methods with projection methods*, J. Comput. Phys., 229 (2010), pp. 2479–2496.
- [13] X. HE AND G. D. DOOLEN, *Lattice Boltzmann method on curvilinear coordinates system: flow around a circular cylinder*, J. Comput. Phys., 134 (1997), pp. 306–315.
- [14] T.-L. HORNG, P.-W. HSIEH, S.-Y. YANG, AND C.-S. YOU, *A simple direct-forcing immersed boundary projection method with prediction-correction for fluid-solid interaction problems*, Comput. Fluids, 176 (2018), pp. 135–152.
- [15] C. JI, A. MUNJIZA, AND J. J. R. WILLIAMS, *A novel iterative direct-forcing immersed boundary method and its finite volume applications*, J. Comput. Phys., 231 (2012), pp. 1797–1821.
- [16] T. KAJISHIMA, S. TAKIGUCHI, H. HAMASAKI, AND Y. MIYAKE, *TURBULENCE STRUCTURE OF PARTICLE-LADEN FLOW IN A VERTICAL PLANE CHANNEL DUE TO VORTEX SHEDDING*, JSME International Journal, Series B, 44 (2001), pp. 526–535.
- [17] T. KAJISHIMA AND S. TAKIGUCHI, *Interaction between particle clusters and particle-induced turbulence*, Int. J. Heat Fluid Flow, 23 (2002), pp. 639–646.
- [18] T. KAJISHIMA AND K. TAIRA, *Computational Fluid Dynamics: Incompressible Turbulent Flows*, Springer International Publishing AG, 2017.
- [19] K. KHANAFER AND S. M. AITHAL, *Laminar mixed convection flow and heat transfer characteristics in a lid driven cavity with a circular cylinder*, Int. J. Heat Mass Transfer, 66 (2013), pp.

- 200–209.
- [20] J. KIM AND H. CHOI, *An immersed-boundary finite-volume method for simulations of heat transfer in complex geometries*, KSME International Journal, 18 (2004), pp. 1026–1035.
 - [21] J. KIM, D. KIM, AND H. CHOI, *An immersed-boundary finite-volume method for simulations of flow in complex geometries*, J. Comput. Phys., 171 (2001), pp. 132–150.
 - [22] C.-C. LIAO, Y.-W. CHANG, C.-A. LIN, AND J. M. MCDONOUGH, *Simulating flows with moving rigid boundary using immersed-boundary method*, Comput. Fluids, 39 (2010), pp. 152–167.
 - [23] H. LUO, H. DAI, P. J. S. A. FERREIRA DE SOUSA, AND B. YIN, *On the numerical oscillation of the direct-forcing immersed-boundary method for moving boundaries*, Comput. Fluids, 56 (2012), pp. 61–76.
 - [24] R. MITTAL AND G. IACCARINO, *Immersed boundary methods*, Ann. Rev. Fluid Mech., 37 (2005), pp. 239–261.
 - [25] J. MOHD-YUSOF, *Combined immersed-boundary/B-spline methods for simulations of flows in complex geometries*, Annual Research Briefs 1997, pp. 317–327, Center for Turbulence Research, NASA Ames/Stanford University, Stanford, CA.
 - [26] K. NAGENDRA, D. K. TAFTI, AND K. VISWANATH, *A new approach for conjugate heat transfer problems using immersed boundary method for curvilinear grid based solvers*, J. Comput. Phys., 267 (2014), pp. 225–246.
 - [27] D. Z. NOOR, M.-J. CHERN, AND T.-L. HORNG, *An immersed boundary method to solve fluid-solid interaction problems*, Comput. Mech., 44 (2009), pp. 447–453.
 - [28] J. R. PACHECO, A. PACHECO-VEGA, T. RODIĆ, AND R. E. PECK, *Numerical simulations of heat transfer and fluid flow problems using an immersed-boundary finite-volume method on non-staggered grids*, Numerical Heat Transfer, Part B, 48 (2005), pp. 1–24.
 - [29] A. PACHECO-VEGA, J. R. PACHECO, AND T. RODIĆ, *A general scheme for the boundary conditions in convective and diffusive heat transfer with immersed boundary methods*, Transactions of the ASME, Journal of Heat Transfer, 129 (2007), pp. 1506–1516.
 - [30] C. S. PESKIN, *Flow patterns around heart valves: a numerical method*, J. Comput. Phys., 10 (1972), pp. 252–271.
 - [31] C. S. PESKIN, *The immersed boundary method*, Acta Numerica, 11 (2002), pp. 479–517.
 - [32] W. REN, C. SHU, AND W. YANG, *An efficient immersed boundary method for thermal flow problems with heat flux boundary conditions*, Int. J. Heat Mass Transfer, 64 (2013), pp. 694–705.
 - [33] Y.-H. TSENG AND J. H. FERZIGER, *A ghost-cell immersed boundary method for flow in complex geometry*, J. Comput. Phys., 192 (2003), pp. 593–623.
 - [34] M. TYAGI AND S. ACHARYA, *Large eddy simulation of turbulent flows in complex and moving rigid geometries using the immersed boundary method*, Int. J. Numer. Methods Fluids, 48 (2005), pp. 691–722.
 - [35] M. UHLMANN, *An immersed boundary method with direct forcing for the simulation of particulate flows*, J. Comput. Phys., 209 (2005), pp. 448–476.
 - [36] M. VANELLA, P. RABENOLD, AND E. BALARAS, *A direct-forcing embedded-boundary method with adaptive mesh refinement for fluid-structure interaction problems*, J. Comput. Phys., 229 (2010), pp. 6427–6449.
 - [37] Y. WANG, C. SHU, L. M. YANG, *Boundary condition-enforced immersed boundary-lattice Boltzmann flux solver for thermal flows with Neumann boundary conditions*, J. Comput. Phys., 306 (2016), pp. 237–252.
 - [38] Z. WANG, J. FAN, AND K. LUO, *Combined multi-direct forcing and immersed boundary method for simulating flows with moving particles*, Int. J. Multiphase Flow, 34 (2008), pp. 283–302.

- [39] J.-S. YOO, *Dual free-convective flows in a horizontal annulus with a constant heat flux wall*, Int. J. Heat Mass Transfer, 46 (2003), pp. 2499–2503.
- [40] N. ZHANG AND Z. C. ZHENG, *An improved direct-forcing immersed-boundary method for finite difference applications*, J. Comput. Phys., 221 (2007), pp. 250–268.
- [41] N. ZHANG, Z. C. ZHENG, AND S. ECKELS, *Study of heat-transfer on the surface of a circular cylinder in flow using an immersed-boundary method*, Int. J. Heat Fluid Flow, 29 (2008), pp. 1558–1566.